Highly porous Fe_2O_3-SiO_2 layer for acoustic wave based H_2S sensing: mass loading or elastic loading effects?

Junsen Wang[a], Jian Che[a], Changcang Qiao[a], Ben Niu[a], Wenting Zhang[a], Yucheng Han[b], Yongqing Fu[c], Yongliang Tang[a,*]

[a]School of Physical Science and Technology, Southwest Jiaotong University, Chengdu, 610031, People's Republic of China

[b]School of Physics, University of Electronic Science and Technology of China, Chengdu, 610054, People's Republic of China

[c]Faculty of Engineering and Environment, Northumbria University, Newcastle upon Tyne, NE1 8ST, UK

*Correspondance to Yongliang Tang. Email: tyl@swjtu.edu.cn Tel:86-15884573263

Abstract

A highly porous Fe_2O_3-SiO_2 layer prepared using sol-gel and spin-coating methods was applied on the surface of a surface acoustic wave (SAW) device for H_2S sensing. SiO_2 in this sensing layer serves as a porous support for dispersing Fe_2O_3 nanoparticles, and Fe_2O_3 nanoparticles can effectively adsorb and react with H_2S molecules. By changing the Fe/Si molar ratio in this Fe_2O_3-SiO_2 layer, its pore volume, pore distribution and H_2S adsorption capacity can be adjusted, the contribution of mass loading effect and the elastic loading effect toward the frequency response of the sensor can be controlled, and the sensing performance of the sensor can be optimized. The optimized sensing response is -4.4 kHz toward 100 ppm H_2S, with a good selectivity and reproducibility operated at room temperature (25 °C).

Keywords: SAW sensor; H_2S; Fe_2O_3-SiO_2; Mass loading; Elastic loading

1. Introduction

Hydrogen sulfide (H_2S) is highly flammable and toxic, and exists in sewers, well water, oil and gas wells and volcanoes [1]. Because of its higher density than that of air, H_2S is often accumulated in low grounds and enclosed spaces, such as manholes and underground warehouses [2,3], which causes potential hazards. Influence of H_2S on human health depends on the its concentration and exposure time. For example, H_2S gas with a concentration of 25 ppm can stimulate the trachea or conjunctivitis. Whereas with a concentration up to 50 ppm, human olfaction will be paralyzed, which affects human judgment. If its concentration is as high as 400 ppm, people will die within an hour [4]. Even at its low concentrations, the long-time exposure to H_2S gas can do harm to human health, ranging from mild headaches, eye irritation, coma or even death [5,6]. Therefore, it is critical to develop a reliable and highly sensitive H_2S gas sensor.

Surface acoustic wave (SAW) sensor has been used for H_2S sensing due to its high sensitivity, fast response, high accuracy, low cost, real-time measurement and wireless sensing capabilities [7-9]. The core part of the SAW sensor is a sensitive layer deposited on a conventional SAW resonator [10,11]. Any physical or chemical perturbation on the sensitive layer, such as mass loading, elastic loading, electrical loading, etc., will cause the frequency shift of the SAW resonator. The mass, elastic and electrical loading effects refer to the changes of mass, elastic modulus and conductivity of this sensitive layer caused by the adsorption of the analyte [12]. Many

studies [13-15] showed that key sensing mechanisms of a SAW H_2S sensor are changes of mass and conductivity of the sensitive layer when the sensor is exposed to H_2S gas. For examples, Wang et al. proposed a SnO_2-CuO composite layer, which improved gas sensitivity of SAW H_2S sensors due to both mass loading and electrical loading effects [16]. While our previous work based on a porous ZnO-Al_2O_3 nanocomposite layer showed that the elastic loading effect can also play an important role in the sensing performance of SAW H_2S sensors [9]. Thus, it is reasonable to conclude that all the three effects may have the contribution toward the response of the SAW H_2S gas sensor, just as the results revealed by Raj et al. when studying ammonia sensors [17]. However, there are few studies which have been focused on understanding of synergistic effects among these three factors and further optimizing their effects to enhance the sensing performance of a H_2S sensor.

In this study, we proposed to use a porous Fe_2O_3-SiO_2 nanocomposite layer for H_2S sensing. Fe_2O_3 nanoparticles in this compound layer have a good adsorption capacity for H_2S and can capture and react with H_2S molecules in the environment. While SiO_2 can serve as a porous support [12] for dispersing Fe_2O_3 nanoparticles in the layer, which effectively allows H_2S molecules to diffuse into this layer and interact with Fe_2O_3 nanoparticles. By changing the content ratio of Fe/Si in this layer, total pore and micropore volumes of the layer and the adsorption capacity of the layer for H_2S can be adjusted [18]. In addition, large porosity of the sensitive layer is found to be beneficial for the mass loading and electrical loading effects while micropores in the layer account for the elastic loading effect [19,20]. Therefore, the contributions of

different factors to the responses of the sensor can be controlled and optimized by adjusting the Fe/Si molar ratio in the layer, and the sensing mechanisms can be fully understood.

2. Experimental details

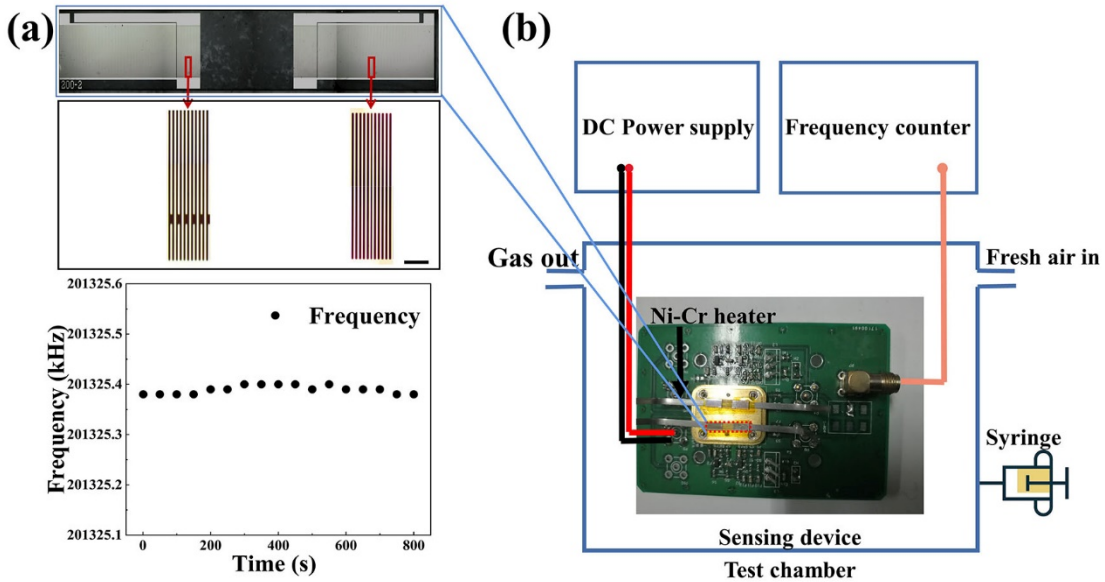

Fig. 1. (a) Schematic illustrations of a SAW resonator and its central frequency. The scale bar is 50 μm; (b) The schematic of experimental setup for gas sensing measurement.

ST-cut quartz SAW resonators with the center frequency of ~201 MHz had the same structure as reported in our previous publication [9] (Fig. 1(a)). The Fe_2O_3-SiO_2 composite layer was prepared by using a sol-gel method. The Stöber method was used to prepare silica sol [21], which had a concentration of 0.5 mol/L. Fe_2O_3 sol was prepared by dissolving $FeCl_3$ in deionized water under magnetic stirring and then aged for 24 h at room temperature. The concentration of the obtained Fe_2O_3 sol was 0.25 mol/L. The Fe_2O_3 sol and silica sol were added into a beaker with Fe/Si molar ratios of 1:9, 2:8 and 3:7, respectively. The mixed sol was stirred for 1 h to obtain a homogeneous solution, and then aged for 24 h. For preparing the composite layer on the SAW device, the mixed sol was spin-coated onto the SAW resonator at a speed of

4000 r/min for 30 s. Then, the coated SAW resonator was immediately annealed in air at 400 °C for 2 h to form a Fe_2O_3-SiO_2 composite layer. For convenience, the Fe_2O_3-SiO_2 composite layers with Fe/Si molar ratios of 1:9, 2:8, and 3:7 were named as samples of FS-1, FS-2, FS-3, respectively. The characterization methods for the prepared sensing layers can be found in ref. [9,12].

The annealed resonators were connected to peripheral circuits to build SAW sensors [12]. The experimental set-up for gas sensing measurement is illustrated in Fig. 1(b). The sensing device was put into a gas testing chamber with a volume of 20 L, and then connected to a frequency counter (Agilent 53132A) to record the dynamic changes of the resonant frequency of SAW sensor. Heaters were mounted right below the resonators and were used to heat the devices for assisting the recovery of the sensors. The temperature and humidity in the lab environment and testing chamber were controlled at 25 °C and 50% by an air conditioner and a humidity controller and all the sensing measurements were conducted at these temperature and RH unless otherwise specified. High precision gas-tight syringes (Hamilton 1000) were used to collect the testing gases (H_2S, NH_3, SO_2, C_2H_5OH, C_3H_6O gases diluted to 2 vol% in dry air) from gas sampling bags obtained from the NIMTT, China. The collected gas was injected into the testing chamber, and the gas concentration in the chamber was controlled by adjusting the injecting volume. The response of the SAW sensor was defined as $\Delta f = f_s - f_0$, where f_s is the oscillating frequency of the sensor in the test gas mixed in air, and f_0 is the oscillating frequency in the air, respectively. After the responses were recorded, the tested gas was pumped out and pure air was immediately

filled into the chamber to allow the recovery of the sensor.

3. Results and discussion

3.1. Structural characterization

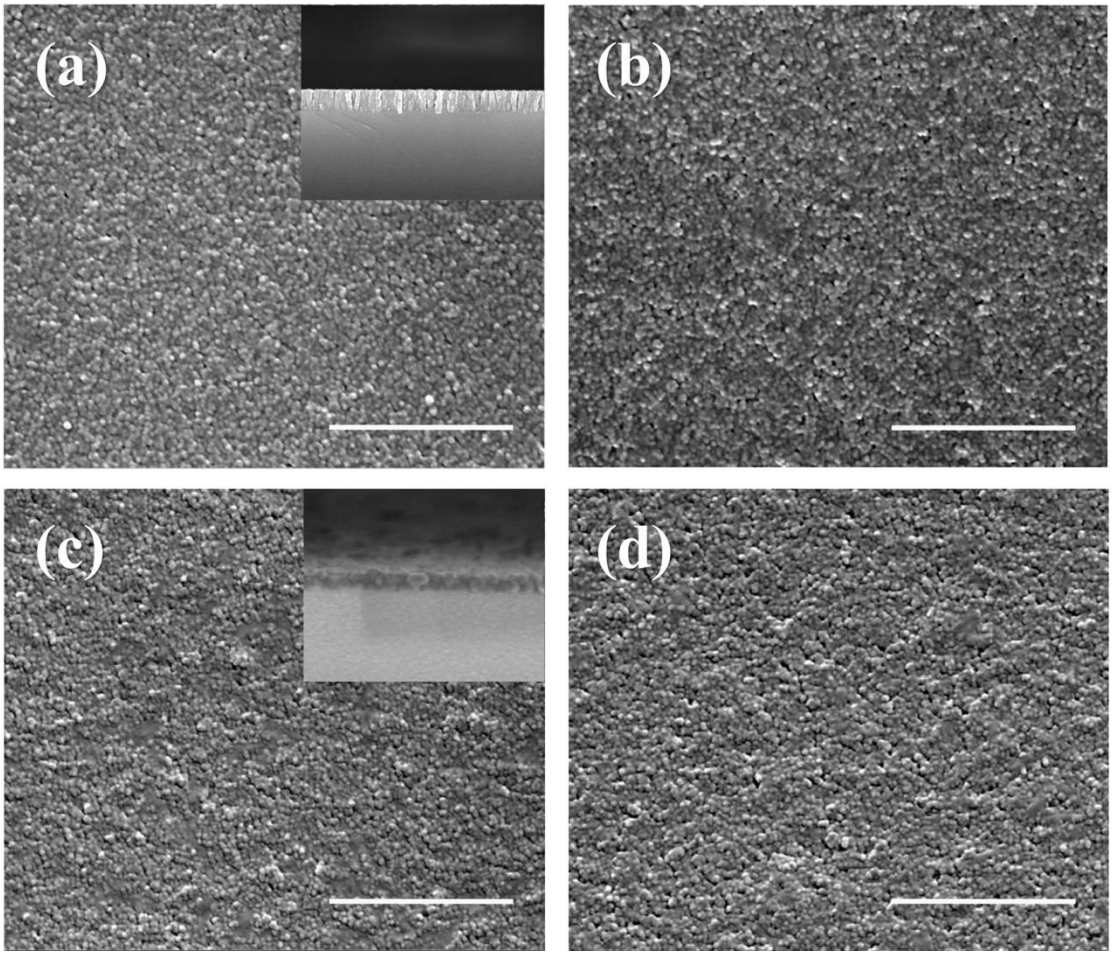

Fig. 2. SEM images of surface morphology for (a) pure SiO_2, (b) FS-1, (c) FS-2 and (d) FS-3 layers. Scale bars in images are 1 μm.

SEM images of the pristine SiO_2 layer and Fe_2O_3-SiO_2 composite sensitive layers are shown in Fig. 2. The SiO_2 layer is uniform, but porous, with an average pore diameter of about 10 nm. The Fe_2O_3-SiO_2 composite layer has a porous structure similar as that of the SiO_2 layer. However, with the increase of Fe_2O_3 proportion, the microstructure of the layer changes and the uniformity of the sensitive layer becomes

worsen. Large scale pores and cracks appear on the layer surface. The inset images in Figs. 2(a) and 2(c) are the cross-sectional morphologies of the pristine SiO_2 and FS-2 layers. The layers of FS-1, FS-2 and FS-3 samples have the similar cross section morphologies. The thickness of the pure SiO_2 layer is ~290 nm and those of the FS-1, FS-2 and FS-3 layers are ~100 nm.

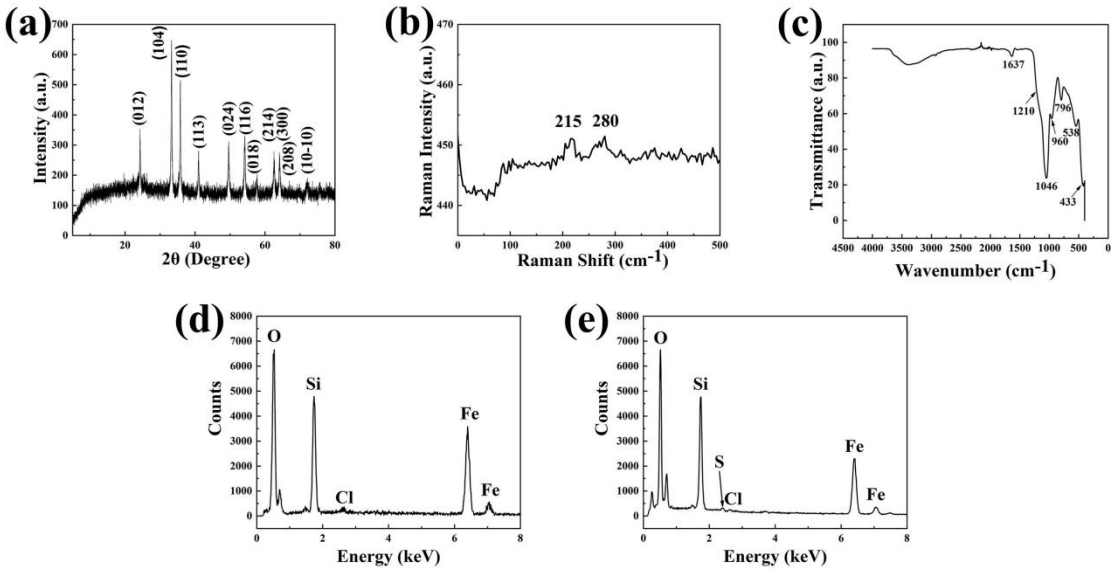

Fig. 3. (a) XRD patterns, (b) Raman spectrum, (c) FTIR spectrum, (d) EDS spectrum of the as-prepared Fe_2O_3-SiO_2 material; (e) EDS spectrum of the as-prepared Fe_2O_3-SiO_2 material after tested with H_2S gas.

Fig. 3(a) shows XRD spectra of the Fe_2O_3-SiO_2 material. The diffraction peaks can be indexed as (012), (104), (110), (113), (024), (116), (018), (214), (300), (208), (10-10) crystal planes of the α-Fe_2O_3. In addition, a broad peak located at about 22° can be also observed, indicating the presence of amorphous SiO_2. Using the Debye-Scherrer's formula [22], the estimated crystal size of Fe_2O_3 in the layer is ~30 nm.

Fig. 3(b) shows Raman spectrum of the Fe_2O_3-SiO_2 material. Two peaks are identified at 215 cm^{-1} and 280 cm^{-1}, which are the characteristic peaks of the A_1g (225

cm^{-1}) and Eg (293 cm^{-1}) modes for the Fe_2O_3 crystals, respectively [23]. The Raman result clearly confirms the presence of Fe_2O_3 in the prepared sensitive layer, which is in consistent with the XRD result.

Fig. 3(c) shows FTIR spectrum of the Fe_2O_3-SiO_2 material. In the high wavenumber spectral range, a wide band between 3600 cm^{-1} and 2800 cm^{-1} can be attributed to the stretching vibration mode of different hydroxyl groups [24]. The band at 1630 cm^{-1} is related to molecular water, and the band at 960 cm^{-1} is attributed to the stretching mode of non-bridging oxygen atoms [25]. The bands at 796 cm^{-1}, 1046 cm^{-1} and the shoulder at 1210 cm^{-1} are related to SiO_2. The bands at 433 cm^{-1} can be attributed to Fe-O bond and 538 cm^{-1} is related to Fe_2O_3 [26], which again indicates Fe_2O_3-SiO_2 nanocomposite layers were successfully prepared.

Fig. 3(d) shows the EDS result of the as-prepared Fe_2O_3-SiO_2 material, in which signals of O, Si, Fe and Cl elements were detected. Among them, Cl signal is from the $FeCl_3$ powder when the preparing Fe_2O_3 sol. The O, Si and Fe element signals are linked with the prepared Fe_2O_3-SiO_2 nanocomposite layer. The Fe_2O_3-SiO_2 material was further sent to EDS characterization immediately after it was tested with H_2S gas. As shown in Fig. 3(e), a slight S peak appears in this spectrum, which indicates that Fe_2O_3 has reacted with H_2S gas molecules to form iron sulfide compound, such as Fe_2S_3, as reported by previous literatures [27-29].

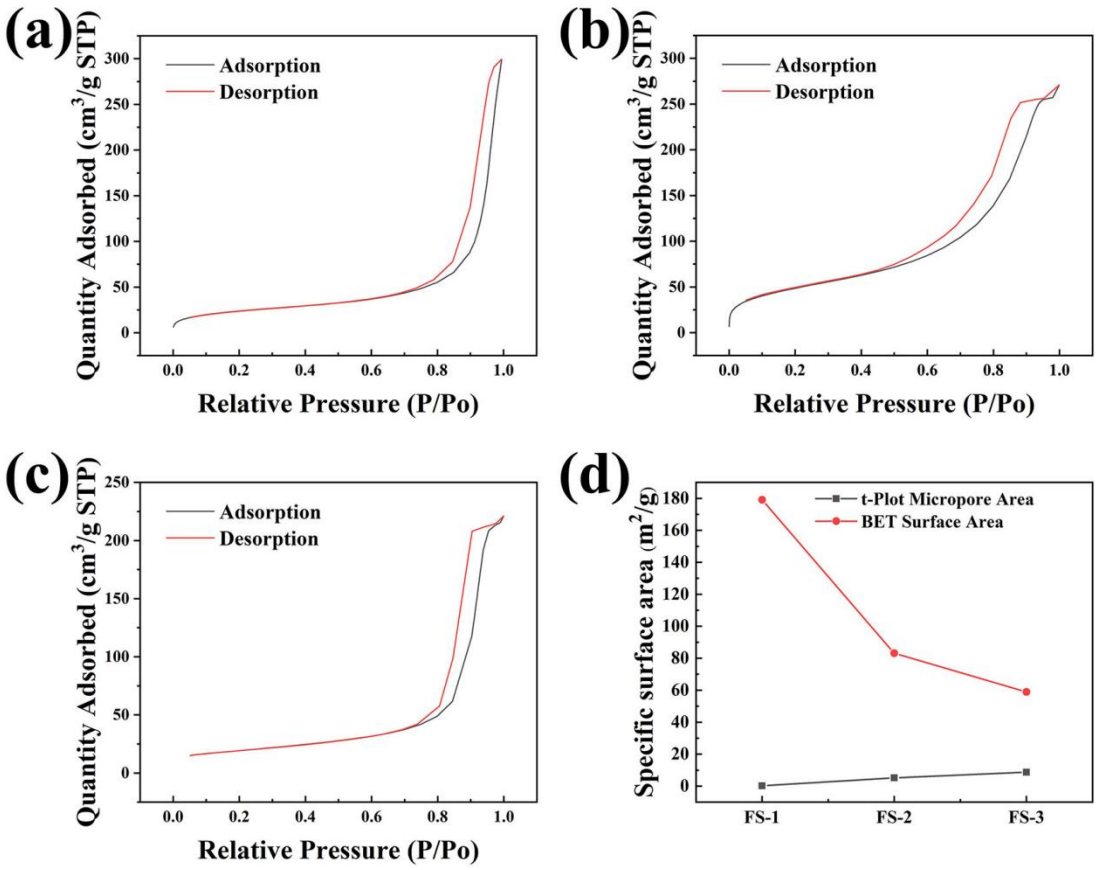

Fig. 4. Nitrogen adsorption and desorption isothermals of the (a) FS-1, (b) FS-2 and (c) FS-3 materials; (d) Micropore areas and total surface areas of the FS-1, FS-2 and FS-3 materials.

Figs. 4(a)-4(c) show the nitrogen gas adsorption and desorption isotherms of FS-1, FS-2 and FS-3 samples. The BET surface areas of the FS-1, FS-2 and FS-3 samples are 179.37 m^2/g, 81.29 m^2/g and 67.60 m^2/g. Whereas the t-Plot micropore areas of the FS-1, FS-2 and FS-3 samples are 0.2609 m^2/g, 5.1472 m^2/g and 8.7366 m^2/g (Fig. 4(d)). The results indicate that with the increase of Fe_2O_3 content, the total pore surface areas and the pore volumes decrease, whereas the surface area and volume of the micropores increase, which are consistent with the SEM results.

3.2. Sensing performance and mechanisms

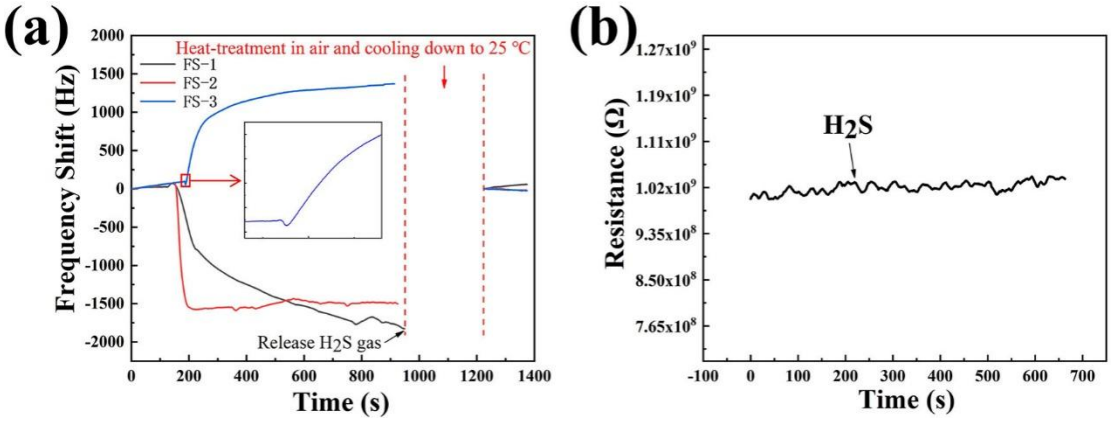

Fig. 5. (a) Dynamic frequency responses of FS-1, FS-2, FS-3 sensors to 4 ppm H_2S at RH = 50% and 25 °C; (b) Resistance response of FS-2 sensor to 20 ppm H_2S gas.

The dynamic frequency responses of sensors to 4 ppm H_2S at RH = 50% and 25 °C are shown in Fig. 5(a). The frequency response of the FS-1 sensor toward H_2S gas is negative, e.g., continues to decrease during the exposure process. When the exposure time of the sensor toward H_2S is 800 s, the response is -1760 Hz. The FS-2 sensor has a negative response, too. However, different from the FS-1 sensor, its response is much faster, but it will become stable within 60 s with a frequency shift of -1570 Hz. Interestingly, the FS-3 sensor initially shows a slightly negative response, then the response becomes positive after a short period of time and then keeps increasing up to 1320 Hz at the exposure time of 800 s. Obviously, these sensors have quite different response curves, which indicates that their sensing mechanisms to H_2S gas may be different.

After 800 s, the H_2S gas was released from the chamber and the sensors were exposed to the fresh air to allow the recovery of the sensors. Nevertheless, none of the sensors can be fully recovered as shown in Fig. 5(a), which may be due to the strong

chemical adsorption of H_2S gas on these layers. By heating the resonators in the air at 200 °C for 5 min, and then cooling naturally down to room temperature, the sensors can all be recovered, indicating that the H_2S molecules adsorbed by the layer has completely been removed during this high temperature treatment process.

The frequency response of a SAW gas sensor is mainly induced by three mechanisms, i.e., mass loading effect, elastic loading effect and electrical loading effect of the sensitive layer [19,20]. The relationship between the frequency response (Δf) and the mass change of the layer is as follows [30]:

$$\Delta f = (k_1 + k_2) \times f_0^2 \times \Delta m \quad (1)$$

where k_1=-8.7× 10^{-8} m^2skg^{-1} and k_2=-3.9×10^{-8} m^2skg^{-1} are the material constant, f_0=201 MHz is the center frequency of the SAW resonator, Δf is the change in the layer mass. Since k_1 and k_2 have negative signs, an increase in the mass will result in a negative frequency response.

The relationship between the frequency response (Δf) and the change in the elastic modulus of the layer is as follows [30]:

$$\Delta f = p\Delta E \quad (2)$$

where p is a positive constant, E is the elastic modulus, and ΔE is the change in the elastic modulus of the layer. Hence, an increase of elastic modulus of the layer will cause a positive frequency response.

The relationship between the frequency response (Δf) and the change in layer's conductivity is as follows [31]:

$$\Delta f = -f_0 \times \frac{K^2}{2} \times \Delta\left(\frac{1}{1+\left(\frac{v_0 C_S}{\sigma_s}\right)^2}\right) \quad (3)$$

where, $K^2 = 0.0011$ is the electromechanical coefficient of the piezoelectric substrate, v_0=3158 ms^{-1} is the undisturbed SAW velocity, C_S=0.5 pFcm^{-1} is the sum of the dielectric constant of the layer and the area above the substrate, and σ_s is the conductivity of the sensitive layer.

Fig. 5(b) shows the resistance responses of the FS-2 sensor exposed to 20 ppm H_2S gas. The resistance does not change, indicating there is no obvious change in σ_s. Hence, the electrical loading effect can be neglected according to the Equation 3. Therefore, we can assume that the frequency response of the sensors is mainly contributed from changes in mass and elastic modulus of layers, i.e. mass and elastic loading effects.

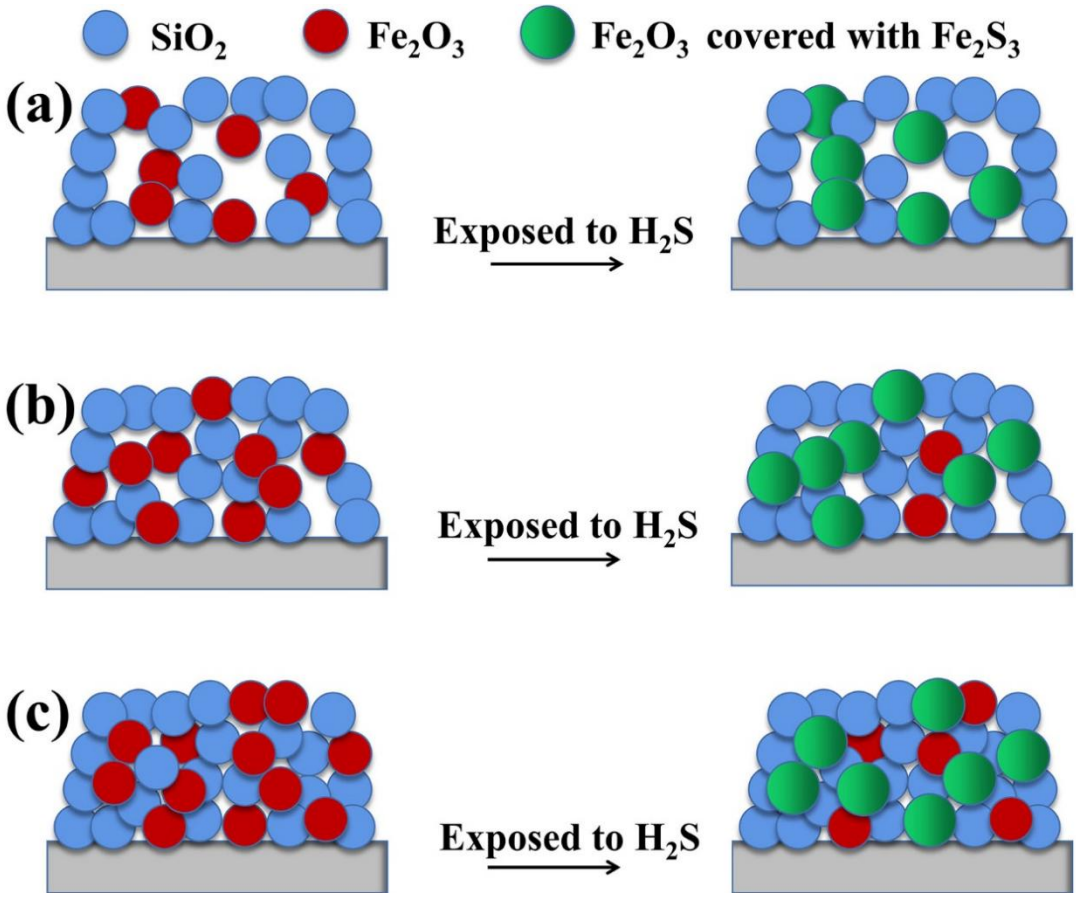

Fig. 6. Schematic diagram of sensing mechanism of (a) FS-1, (b) FS-2 and (c) FS-3 sensors.

The changes in the mass and modulus of the layer are caused by the adsorption of H_2S molecules in the sensing layer. The Fe_2O_3 nanoparticles in the composite layer have a strong adsorption capacity for H_2S molecules and generate sulfides (Fe_2S_3) as shown in Fig. 6. According the EDS results and references [27-29], the reaction between Fe_2O_3 and H_2S can be written as follows:

$$\mathrm{Fe}_2O_3 + 3\mathrm{H}_2S \rightarrow Fe_2S_3 + 3\mathrm{H}_2O \quad (4)$$

This formed Fe_2S_3 layer (based on Equation 4) covers the surface of the Fe_2O_3 particles. As it is well-known, the Fe_2S_3 has a higher molar mass than that of Fe_2O_3, which results in an increase of the overall mass of the layer after this chemical reaction. While the relative density of newly formed Fe_2S_3 is 4.3 g/cm^3 is lower than the density of Fe_2O_3 (5.24 g/cm^3). When the Fe_2S_3 layers with a higher mass but a lower density cover over the Fe_2O_3 nanoparticles, the particles' total volumes are increased significantly. Therefore, the total pore volume in the layer shrinks, resulting in an increase in the elastic modulus of the layer [17,18]. According to Equations (1) and (2), the increase in the mass and elastic modulus of the layer caused by the formation of Fe_2S_3 will lead to the negative and positive frequency responses of the SAW sensor, respectively.

Fig. 5(a) shows that the sensing layer cannot be spontaneously recovered to its initial state after the reactions and then exposure to the atmosphere at room temperature. This is mainly because the reaction rate between Fe_2S_3 and O_2 (Equation

5) is slow at room temperature [30]. However, this can be accelerated at a higher temperature of 200 °C.

$$2Fe_2S_3 + 9O_2 \rightarrow 2Fe_2O_3 + 6SO_2 \quad (5)$$

Based on the above discussions, both the mass loading and elastic loading effects contribute to the frequency responses of the sensors. However, as shown in Fig. 5(a), the sensors of FS-1, FS-2, and FS-3 have different response characteristics to H_2S. This can be linked to the different microstructures of the sensing layers [19,20]. According to the BET and SEM results, an increase in Fe_2O_3 content results in a decrease of the total pore volume but an increase of micropore volume (Fig. 2 and Fig. 4). Previous studies revealed that the larger volume of pores is beneficial for the diffusion of gas into the sensing layer, which helps the interactions between the layer and gas molecules [32]. While the changes of micropore volumes accounts for the change of the elastic modulus the sensing layer [9].

For example, the FS-1 sensing layer has the lowest Fe_2O_3 content, hence the largest total pore but the smallest micropore volumes. When it is exposed to H_2S gas, H_2S molecules diffuse into and react with the sensing layer to produce abundant Fe_2S_3, which leads to a considerable increase in the mass of the layer and a slight decrease of micropore volume (i.e. slight increase in the elastic modulus). Therefore, the mass variation in the layer results in a significantly negative response of the sensor (Fig. 5(a), the black line).

Compared with the FS-1 layer, the FS-2 layer has moderate amounts of Fe_2O_3, which leads to the moderate total pore and micropore volumes (Fig. 6(b)). Thus, the

reaction between H_2S molecules and the sensing layer will cause a less significant increase of the mass but a more prominent elastic modulus in the layer compared with the FS-1 one. Therefore, there is a competition between the negative and positive frequency shifts of the SAW sensor caused by mass and elastic loading effects, respectively. Thus, a final moderate negative frequency response can be observed (Fig. 5(a), the red line).

Contrary to the FS-1 layer, the FS-3 layer has the smallest total pores but largest micropore volumes (Fig. 6(c)), thus results in the strongest positive frequency of the sensor (Fig. 5(a), the blue line). In addition, it is worth noting that this response curve shows an initial decrease trend but a later increase trend of frequency changes (the inset in Fig. 5(a)). This again clearly reveals the existence of a competition between the mass and elastic loading effects.

Based on above discussion, it can be concluded that the sensing performance of a SAW gas sensor can be optimized by adjustment of the contribution of the different effects through rational design of pore distribution of the sensitive layer.

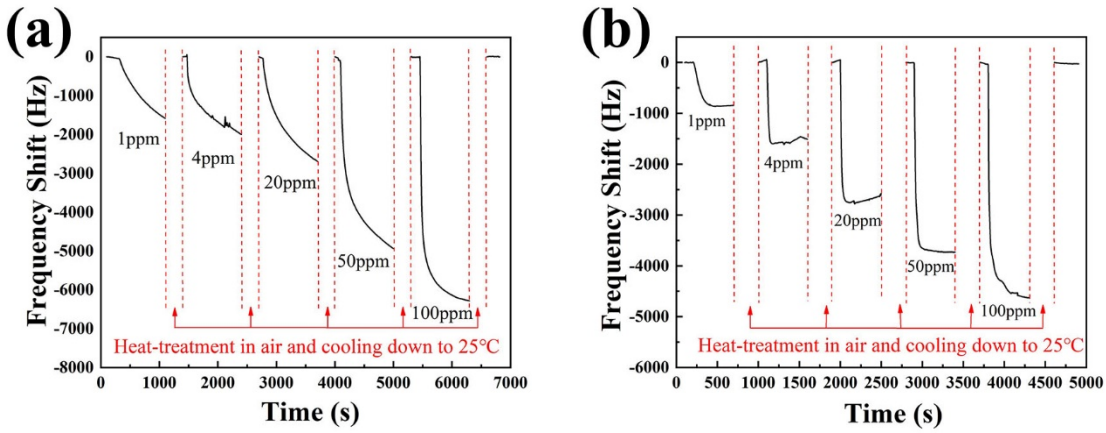

Fig. 7. Dynamic frequency responses of (a) FS-1 and (b) FS-2 sensors to H_2S with different concentrations.

The FS-1 sensor has the strongest frequency response, while the FS-2 sensor has the fastest response, so these two sensors were chosen to conduct the further gas sensing measurements. The dynamic responses of the sensors to H_2S molecules with different concentrations (1, 4, 20, 50, 100 ppm) are shown in Fig. 7. For the FS-1 sensor, the exposure time of the sensor to H_2S gas is ~1000 s, while it is 500 s for the FS-2 sensor because of the fast response. The responses of both sensors become stronger as the concentration of H_2S molecules increases. At a low concentration of 1 ppm H_2S, the frequency shift of the sensor with FS-1 and FS-2 layers are -1500 Hz and -800 Hz. As the concentration of H_2S increases up to a level of 100 ppm, the frequency shifts of the sensor with FS-1 and FS-2 layers reach -6200 Hz and -4400 Hz, respectively. The frequency response and response time as functions of the H_2S concentration are shown in Fig. 8(a), which reveals that the sensor with the FS-1 sensing layer has a much stronger response while the sensor with the FS-2 sensing layer has a much better linearity and a faster response. The response times of the sensor with the FS-2 sensing layer are all below 200 s within the concentration range of 1-100 ppm. The recovery of sensors is very slow at room temperature as discussed before (Fig.7).

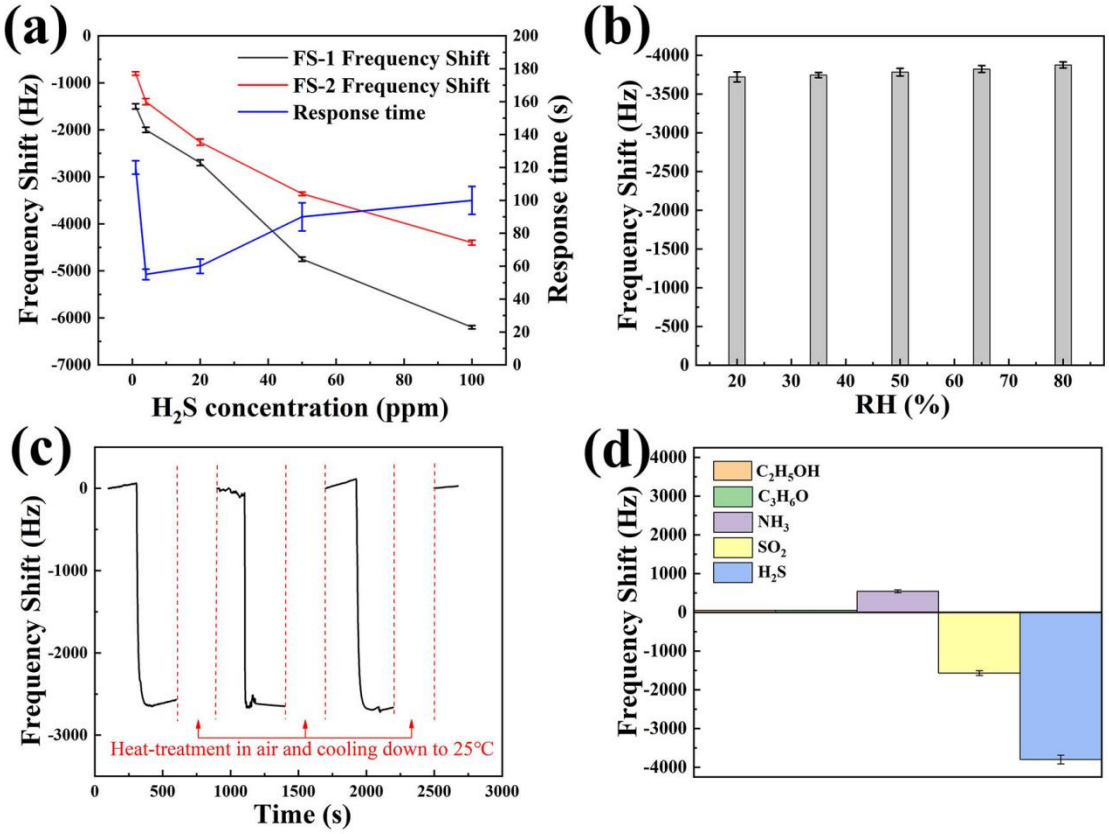

Fig. 8. (a) The response and response time of the FS-1 and FS-2 sensors as functions of the H_2S concentration; (b) the response of the FS-2 sensor to 50 ppm H_2S with various RH at room temperature; (c) Dynamic response of the FS-2 sensor to 20 ppm H_2S gas for 3 consecutive cycles; (d) the response of the FS-2 sensor to 50 ppm SO_2, C_2H_5OH, C_3H_6O, NH_3 and H_2S gases.

Humidity resistance is a critical parameter for a good gas sensor. The influence of the humid condition on the H_2S response of the FS-2 sensor was measured under RH of 20%, 35%, 50%, 65% and 80% at 25 °C. As shown in Fig. 8(b), the sensor's response changes little with the increase in RH value, indicating the good humidity resistance of the sensor. Good reproducibility is also critical for a practical gas sensor. The reproducibility of the FS-2 sensor was examined by exposing the sensor to 20 ppm H_2S for 3 consecutive cycles in an environment of RH = 50% and 25 °C. As the

results shown in Fig. 8(c), the sensor showed similar responses in the concessive experimental cycles, indicating the excellent reproducibility of the sensor.

The selectivity of the FS-2 sensor was also evaluated by examining the responses of the sensor toward different gases including C_2H_5OH, C_3H_6O, SO_2 and NH_3. As shown in Fig. 8(d), the sensor has no obvious responses to 50 ppm C_2H_5OH and C_3H_6O. A positive response to 50 ppm NH_3 and a negative response to 50 ppm SO_2 can be observed. However, the responses to SO_2 and NH_3 are significantly weaker than that to H_2S, indicating the good selectivity of the sensor, which can be attributed to the good adsorption capacity of Fe_2O_3 for H_2S [33].

4. Conclusions

SAW gas sensors based on porous sol-gel Fe_2O_3-SiO_2 sensing layers were fabricated and their H_2S sensing performance was studied. SiO_2 in the layer serves as porous support for dispersing Fe_2O_3 nanoparticles, which can effectively adsorb and react with H_2S. Increasing Fe/Si molar ratio of the layer results in the decrease of the total pore but increase in micropore volumes, which leads to the degradation of mass loading effect and the enhancement of elastic loading effect. Consequently, the frequency response of the SAW sensor caused by the competitions of these two effects can be optimized by rational control the Fe/Si ratio of the composite layer and thus the pore distribution of in the layer. For the sensor based on the layer with the Fe/Si ratio of 2:8, it has a fast response of -4.4 kHz to 100 ppm H_2S gas, as well as excellent reproducibility and selectivity.

Acknowledgments

This work was supported by the National Natural Science Foundation of China (11805158, 61178018), and the Engineering Physics and Science Research Council of UK (EPSRC EP/P018998/1).

References

[1] L.A. Montoya, M.D. Pluth, Selective turn-on fluorescent probes for imaging hydrogen sulfide in living cells, Chem. Commun. 48 (2012) 4767-4769.

[2] D.C. Glass, A review of the health effects of hydrogen sulphide exposure, Ann. Occup. Hyg. 34 (1990) 323-327.

[3] J. Miyoshi, E.B. Chang, The gut microbiota and inflammatory bowel diseases, Transl. Res. 179 (2017) 38-48.

[4] S.L. Malone Rubright, L.L. Pearce, J. Peterson, Nitric Oxide-Biol. chem. 71 (2017) 1-13.

[5] K. Eto, T. Asada, K. Arima, T. Makifuchi, H. Kimura, Brain hydrogen sulfide is severely decreased in Alzheimer's disease, Biochem. Bioph. Res. Commun. 293 (2002) 1485-1488.

[6] O. Kabil, R. Banerjee, Redox biochemistry of hydrogen sulfide, J. Biol. Chem. 285 (2010) 21903-21907.

[7] D. Li, X. Zu, D. Ao, Q. Tang, Y. Fu, Y. Guo, K. Bilawal, M.B. Faheem, L. Li, S. Li, Y. Tang, High humidity enhanced surface acoustic wave (SAW) H_2S sensors based on sol-gel CuO films, Sens. Actuators B Chem. 294 (2019) 55-61.

[8] D. Li, Y. Tang, D. Ao, X. Xiang, S. Wang, X. Zu, Ultra-highly sensitive and selective H_2S gas sensor based on CuO with sub-ppb detection limit, Int. J. Hydrogen energy 44 (2019) 3985-3992.

[9] Y. Tang, X. Xu, S. Han, C. Cai, H. Du, H. Zhu, X. Zu, Y. Fu, ZnO-Al_2O_3 nanocomposite as a sensitive layer for high performance surface acoustic wave H_2S

gas sensor with enhanced elastic loading effect, Sens. Actuators B Chem. 304 (2019) 127395.

[10] L. Rana, R. Gupta, M. Tomar, V. Gupta, ZnO/ST-quartz SAW resonator: an efficient NO_2 gas sensor, Sens. Actuators B Chem. 252 (2017) 840-845.

[11] W. Wang, S. He, S. Li, M. Liu, Y. Pan, Enhanced sensitivity of SAW gas sensor coated molecularly imprinted polymer incorporating high frequency stability oscillator, Sens. Actuators B Chem. 125 (2007) 422-427.

[12] Y. Tang， Z. Li， J. Ma， L. Wang， J. Yang， B. Du， Q. Yu， X. Zu, Highly sensitive surface acoustic wave (SAW) humidity sensors based on sol–gel SiO_2 films: Investigations on the sensing property and mechanism, Sens. Actuators B Chem. 215 (2015) 283-291.

[13] W. Luo, J. Deng, Q. Fu, D. Zhou, Y. Hu, S. Gong, Z. Zheng, Nanocrystalline SnO_2 film prepared by the aqueous sol–gel method and its application as sensing films of the resistance and SAW H_2S sensor, Sens. Actuators B Chem. 217 (2015) 119-128.

[14] W. Luo, Q. Fu, D. Zhou, J. Deng, H. Liu, G. Yan, A surface acoustic wave H_2S gas sensor employing nanocrystalline SnO_2 thin film, Sens. Actuators B Chem. 176 (2013) 746-752.

[15] J.D. Galipeau, R.S. Falconer, J.F. Vetelino, J.J. Caron, E.L. Wittman, M.G. Schweyer, J.C. Andle, Theory, design and operation of a surface acoustic wave hydrogen sulfide microsensor, Sens. Actuators B Chem. 24 (1995) 49-53.

[16] X. Wang, W. Wang, H. Li, C. Fu, Y. Ke, S. He, Development of a SnO_2/CuO-

coated surface acoustic wave-based H_2S sensor with switch-like response and recovery, Sens. Actuators B Chem. 169 (2012) 10-16.

[17] V.B. Raj, H. Singh, A.T. Nimal, M. Tomar, M.U. Sharma, V. Gupta, Effect of metal oxide sensing layers on the distinct detection of ammonia using surface acoustic wave (SAW) sensors, Sens. Actuators B Chem. 187 (2013) 563-573.

[18] S.L. Hietala, V.M. Hietala, C.J. Brinker, Dual SAW sensor technique for determining mass and modulus changes, IEEE Trans. Ultrason. Ferroelec. Freq. Control 48 (2001) 262-267.

[19] V.B. Raj, A.T. Nimal, Y. Parmar, M.U. Sharma, V. Gupta, Investigations on the origin of mass and elastic loading in the time varying distinct response of ZnO SAW ammonia sensor, Sens. Actuators B Chem. 166 (2012) 576-585.

[20] V.B. Raj, H. Singh, A.T. Nimal, M.U. Sharma, M. Tomar, V. Gupta, Distinct detection of liquor ammonia by ZnO/SAW sensor: study of complete sensing mechanism, Sens. Actuators B Chem. 238 (2017) 83-90.

[21] W. Stöber, A. Fink, E. Bohn, Controlled growth of monodisperse silica spheres in the micron size range, J. Colloid Interf. Sci. 26 (1968) 62-69.

[22] U. Holzwarth, N. Gibson, The Scherrer equation versus the 'Debye-Scherrer equation', Nat. Nanotechnol. 6 (2011) 534.

[23] S. Onari, T. Arai, K. Kudo, Infrared lattice vibrations and dielectric dispersion in α−Fe_2O_3, Phys. Rev. B 16 (1977) 1717.

[24] M. Burgos, M. Langlet, Condensation and densification mechanism of sol-gel TiO_2 layers at low temperature, Sol-Gel Sci. Technol. 16 (1999) 267-276.

[25] N. Primeau, C. Vautey, M. Langlet, The effect of thermal annealing on aerosol-gel deposited SiO_2 films: a FTIR deconvolution study, Thin Solid Films 310 (1997) 47-56.

[26] F.J.M. Chartier, S.P. Blais, M. Couture, A weak Fe–O bond in the oxygenated complex of the nitric-oxide synthase of Staphylococcus aureus, J. Biol. Chem. 281 (2006) 9953-9962.

[27] C.-Y. Kim, A.A. Escuadro, M.J. Bedzyk, Interaction of H_2S with α-Fe_2O_3(0 0 0 1) surface, Surf. Sci. 601 (2007) 4966-4970.

[28] Y. Teng, X. Zhang, T. Xu, Z. Deng, Y. Xu, L. Huo, S. Gao, A spendable gas sensor with higher sensitivity and lowest detection limit towards H_2S: Porous α-Fe_2O_3 hierarchical tubule derived from poplar branch, Chem. Eng. J. 392 (2020) 123679.

[29] V. Balouria, A. Kumar, S. Samanta, A. Singh, A.K. Debnath, A. Mahajan, R.K. Bedi, D.K. Aswal, S.K. Gupta, Nano-crystalline Fe_2O_3 thin films for ppm level detection of H_2S, Sens. Actuators B chem. 181 (2013) 471-478.

[30] D.S. Ballantine, R.M. White, S.J. Martin, A.J. Ricco, E.T. Zellers, G.C. Fry-e, H . Wohltjen, Acoustic Wave Sensors: Theory, Design, and Physico-Chemical App lications, Academic Press (1997).

[31] A.J. Ricco, S.J. Martin, T.E. Zipperian, Surface acoustic wave gas sensor based on film conductivity changes, Sens. Actuators 8 (1985) 319-333.

[32] T. Kida, S. Fujiyama, K. Suematsu, M. Yuasa, K. Shimanoe, Pore and Particle Size Control of Gas Sensing Films Using SnO_2 Nanoparticles Synthesized by Seed-Mediated Growth: Design of Highly Sensitive Gas Sensors, J. Phys. Chem. C 117

(2013) 17574–17582.

[33] C. Liu, Y. Wang, P. Zhao, W. Li, Q. Wang, P. Sun, X. Chuai, G. Lu, Porous α-Fe_2O_3 microflowers: Synthesis, structure, and enhanced acetone sensing performances, J. Colloid Interf. Sci. 505 (2017) 1039-1046.